PAPER

Improving the Josephson energy in high-Tc superconducting junctions for ultra-fast electronics

Recent citations

- Josephson coupling in high-Tc superconducting junctions using ultra-thin BaTiO3 barriers
H. Navarro *et al*

To cite this article: H Navarro *et al* 2020 *Nanotechnology* **31** 105701

View the article online for updates and enhancements.

This content was downloaded from IP address 181.117.38.97 on 09/03/2021 at 17:18

IOP Publishing Nanotechnology
Nanotechnology 31 (2020) 105701 (6pp) https://doi.org/10.1088/1361-6528/ab59f7

Improving the Josephson energy in high-Tc superconducting junctions for ultra-fast electronics

H Navarro[1,3], **M Sirena**[1,2] **and N Haberkorn**[1,2]

[1] Instituto Balseiro, Universidad Nacional de Cuyo and Comisión Nacional de Energía Atómica, Av. Bustillo 9500, 8400 San Carlos de Bariloche, Argentina
[2] Comisión Nacional de Energía Atómica and Consejo Nacional de Investigaciones Científicas y Técnicas, Centro Atómico Bariloche, Av. Bustillo 9500, 8400 San Carlos de Bariloche, Argentina

E-mail: hnavarro@physics.ucsd.edu

Received 22 July 2019, revised 15 October 2019
Accepted for publication 21 November 2019
Published 16 December 2019

Abstract

We report the electrical transport of thin vertically-stacked Josephson tunnel junctions. The devices were fabricated using 16 nm thick $GdBa_2Cu_3O_{7-\delta}$ electrodes and 1–4 nm $SrTiO_3$ as an insulating barrier. The results show Josephson coupling for junctions with $SrTiO_3$ barriers of 1 and 2 nm. Subtracting the residual current in the Fraunhofer patterns, energies of 3.1 mV and 5.7 mV at 12 K are obtained for STO barriers of 1 nm and 2 nm, respectively. The residual current may be related to the contribution of pinholes and thickness fluctuations in the STO barrier. These values are promising for reducing the influence of thermal noise and increasing the frequency operation rate in superconducting devices using high-temperature superconductors.

Keywords: Josephson junctions, high-Tc superconductor, thin film

(Some figures may appear in colour only in the online journal)

1. Introduction

The development of tunnel Josephson junctions (JJ) is of technological relevance for many applications going from superconducting quantum interference devices (SQUIDS), to radiation detectors and rapid single flux quantum digital electronic circuits [1–5]. Most of them require close-packed arrays of junctions, whose characteristic critical current I_c and normal state resistance R_n have to be uniform over large areas and on large scales from a few to tens of thousands of junctions. The use of high-T_c superconductors (HTS) in JJ, due to the large superconducting gap and operating temperature range [6], offers numerous advantages over other superconducting materials such as Nb [7], nitrides [8] and MgB_2 [9, 10]. The large superconducting gap corresponds to a higher Josephson energy, increasing the devices frequency operation rates, relaxing the cooling requirements and reducing significantly the influence of the thermal noise (I_N) [11]. Most research in JJ based on HTS such as $YBa_2Cu_3O_{7-\delta}$ is oriented to planar arrays developed using ion irradiation [12, 13], edge ramp [14, 15] and bicrystals [16–20]. The design and fabrication of vertically-stacked JJ allows an increased functionality by using barriers with different electronic and magnetic properties. Nevertheless, few reports have been published to this date [21]. The main obstacle for its design is related to the 3D growth mechanism usually observed in HTS thin films. If the electrodes display huge roughness, then thick barriers of several nanometers are required to reduce the influence of pinholes and to have Josephson coupling. Moreover, the performance of JJ is affected by suppression of the properties at the interfaces [22, 23].

In this letter, we report the electrical properties of superconductor/insulator/superconductor (SIS) vertically-stacked tunnel junctions using thin $GdBa_2Cu_3O_7$ (GBCO) as superconducting electrodes and $SrTiO_3$ (STO) as the insulating barrier. GBCO is a superconducting material with critical temperature $T_c \sim 93$ K. STO is a dielectric material [24]

[3] Present Address: Department of Physics and Center for Advanced Nanoscience, University of California, San Diego, La Jolla, CA 92093, United States of America.

 © 2019 IOP Publishing Ltd Printed in the UK

and ferroelectricity (FE) may be induced by strain [25]. GBCO has an orthorhombic structure with lattice parameters of $a = 0.383$ nm, $b = 0.389$ and $c = 1.17$ nm. STO is a cubic perovskite with $a = 0.3905$ nm. The crystalline structure of GBCO/STO/GBCO trilayers was previously discussed in [26]. In our research, the GBCO thickness of 16 nm was selected by considering a trade-off between T_c and the presence of smooth surfaces [22, 26]. The low surface roughness of the electrodes is critical to be able to fabricate JJ with ultra-thin insulating barriers (i.e. with only a few nanometers). The heterostructures display single phase with (00*l*) orientation. The STO surface displays steps which are mainly originated by the roughness of the bottom GBCO electrode (typical 1 unit cell ~1.2 nm) [22]. The barrier thickness displays typical fluctuations of around 1 STO unit cell [26]. In addition to the thickness fluctuations, the properties of the junctions may be affected by the stacking order at the interfaces, oxygen vacancies and by crystalline defects [27, 28]. The electronic homogeneity of the STO barrier as a function of the thickness was previously analyzed in GBCO/STO bilayers by conducting atomic force microscopy at room temperature [29]. Conductivity maps indicate higher values at the borders of 3D defects than in the terraces and a barrier thickness distribution width of 0.8 nm. The T_c of 16 nm thick GBCO films is T_c ~77 K. Moreover, for GBCO/insulator bilayers the T_c value decreases from ~77 to ~ 40 K when the barrier thickness increases from 1 to 4 nm [30]. The reduction in T_c could be related mainly with the stress induced by the substrate and the barrier, probably modifying the oxygen content [31].

2. Experimental

The epitaxial GBCO/STO/GBCO trilayers were grown by sputtering on STO substrates using the conditions previously described in [22, 26]. The dsubstrate temperature was kept at 730 °C in an Ar (90%)/O_2(10%) mixture at a pressure of 400 mTorr. After deposition, the temperature was decreased to 500 °C, and the O_2 pressure was increased to 100 Torr. Finally, the samples were cooled down to room temperature at a rate of 1.5 °C min^{-1}. A 2 nm thick STO buffer layer was introduced to reduce the nucleation of 3D defects in the GBCO bottom electrode [22]. The tunnel junctions design used 16 nm thick GBCO electrodes and a STO barrier with thickness (d_{STO}) of 1, 2, 3, and 4 nm. Wherever used, the notations [G-d_{STO}-G] indicate a GBCO bottom and top electrodes and a STO barrier with thickness d (nm). The results presented in this work correspond to JJ using GBCO electrodes with very thin STO barriers and an area of 400 μm^2. Figure 1 shows a schematic picture of a tunnel junction. Initially the samples are covered with 10 nm thick Ag using sputtering (to protect the surface). The fabrication process includes successive steps of optical lithography and Argon ion milling [32]. The first step includes optical lithography using a positive photoresist to create square pillars (20 μm × 20 μm), followed by ion milling to remove the top GBCO electrode. The second step involves optical

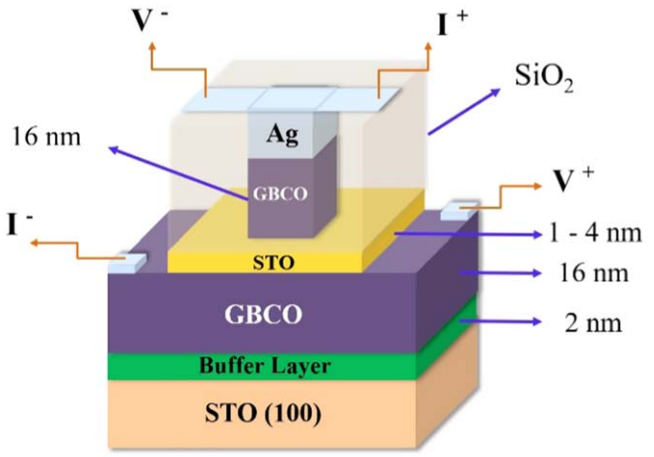

Figure 1. Representative scheme of the materials used in the standard four-point geometry.

lithography using positive photoresist to create square pillars of 10 μm × 210 μm on the center of the pillars generated at the first step. Third, the junction is covered with a 100 nm thick SiO_2 layer by RF sputtering. Finally, the area of 10 μm × 10 μm on the top of the junction is open by lift-off process removing the remaining photoresist using acetone. A path of silver is deposited on the silicon layer to facilitate the electrical connections. Characteristic current–voltage (*IV*) measurements were obtained using the standard four-point geometry in a closed cycle refrigerator with a base temperature of 12 K. The current was applied using a Keithley source. Each point in the curves is the average of 50 measurements. After the change of the current, a 30 s delay time is used before starting with the voltage measurements. A magnetic field **H** parallel to the barrier surface was applied with a copper coil. It is important to note that the ion-milling process described earlier suppresses the T_c at the electrical paths provided by the bottom electrode. For this reason, superconductivity at the bottom electrode is expected only in the area under the junction. The T_c value in trilayers is usually higher than 80 K, being dominated by the transition temperature of the top electrode [30]. In this work, we will define T_c from the Josephson coupling temperature (T_J).

3. Results and discussion

Figure 2 shows typical *IV* curves of JJ with very thin insulator barriers for temperatures ranging from 12 to 100 K. The slope of the *IV* curves (emphasized by the dotted line) corresponds to the normal-state junction resistance R_n. Josephson coupling is observed for STO barriers with thicknesses of 1 and 2 nm. The *IV* curves for [G-3-G] show features related to superconductivity below 35 K, however as we will discuss below, the effect does not correspond to a Josephson coupling. The criteria for I_c determination is indicated in figure 2(b) and corresponds to the departure from the superconducting state (usually abrupt). A low ohmic resistance is observed for [G-2-G], the effect may be related to the silver top layer used to improve the electrical contact at the top electrode (see

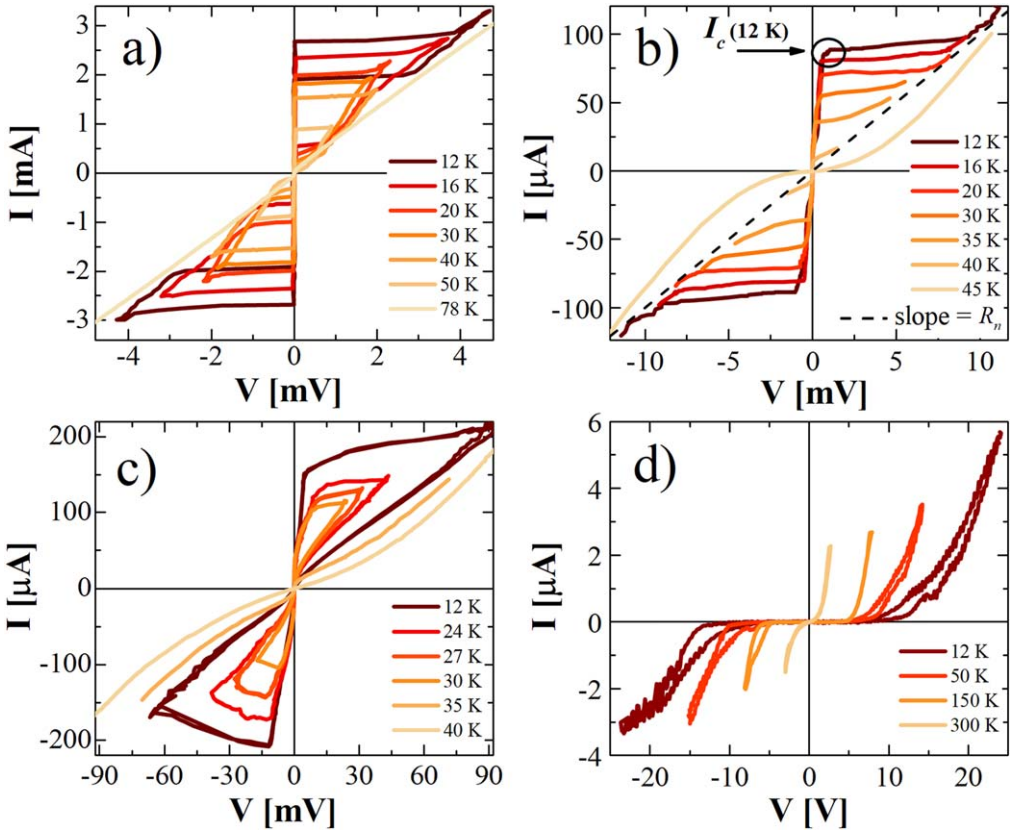

Figure 2. Characteristic *IV* curves at different temperatures for (a) [G-1-G]; (b) [G-2-G]; (c) [G-3-G]; and (d) [G-4-G]. The curves are obtained applying current and measuring voltage. Josephson coupling is observed for JJ with STO barriers of 1 and 2 nm. The criteria for the determination of I_c and R_n are indicated in (b).

figure 1). According with these results, the Josephson coupling appears at thickness similar than the coherence length ξ, which is expected to be between 1 and 2 nm for the GBCO electrodes (as T_c reduces, the ξ increases) [33]. Considering inhomogeneous barriers, the Josephson coupling should be affected by fluctuations in its thickness [34]. Moreover, the effective barrier thickness may be affected by oxygen vacancy migration [28]. The absence of coupling for [G-3-G] and [G-4-G] may be related mainly with an effective thickness larger than ξ. The *IV* curves in [G-4-G] show features usually observed in metal-insulator-metal junctions [26]. The R_n values are 1.6 Ω [G-1-G], 99 Ω [G-2-G] and 550 Ω [G-3-G], indicating a significant increment in the resistance of the junctions when the STO thickness is increased. As expected, increasing the barrier thickness reduces T_J ranging from ∼77 K for [G-1-G] to ∼35 K for [G-3-G]. This effect could be potentiated in these junctions due to the decrease of the T_c with increasing barrier thickness [30]. It is important to note that the *IV* measurements for [G-1-G] show hysteresis, which is usually associated with an underdamped behavior (characteristic of SIS junctions), while the *IV* curves for [G-2-G] do not show hysteresis, corresponding to the overdamped behavior. For the latter, due to a higher Josephson energy, a reduced influence of thermal fluctuations leads to smaller variations in the switching behavior.

In order to verify the presence of Josephson coupling, we investigated the effect of the external magnetic field ***H*** perpendicular to the Josephson current. For that, we performed *IV* measurements applying different magnetic fields (see figures 3(a) and (b)). The Fraunhofer patterns display the expected periodic modulation with minima spacing $\Delta H \sim 30$ G. A distinctive feature of the patterns is a residual current at the minima. This may be interpreted as the presence of short circuits (pinholes) or to an inhomogeneous current density distribution in the junction [35]. Considering thickness fluctuations and effects produced by different interfaces stacking, it is expected that both effects contribute. As we have shown previously for GBCO/STO bilayers, the electrical conductivity at the border of 3D defects is significantly higher than the one in the terraces [29, 30]. If the borders of the 3D defects are pinholes (short circuits), I_c is originated by two contributions: Josephson I_J (terraces) and pinholes I_p (borders of 3D defects). The I_p values for [G-1-G] and [G-2-G] at 12 K (minima 1) are ∼290 μA and ∼30 μA, respectively. According to this scenario, I_J decreases faster than I_p when the STO thickness is increased. This is consistent with our measurements indicating that $I_c \sim I_p$ for [G-3-G] (see below).

The expected field dependence of the I_c for rectangular JJs is given by:

$$I(H) = I_0 \left| \frac{\sin\left(\frac{\pi H}{H_0}\right)}{\frac{\pi H}{H_0}} \right|, \qquad (1)$$

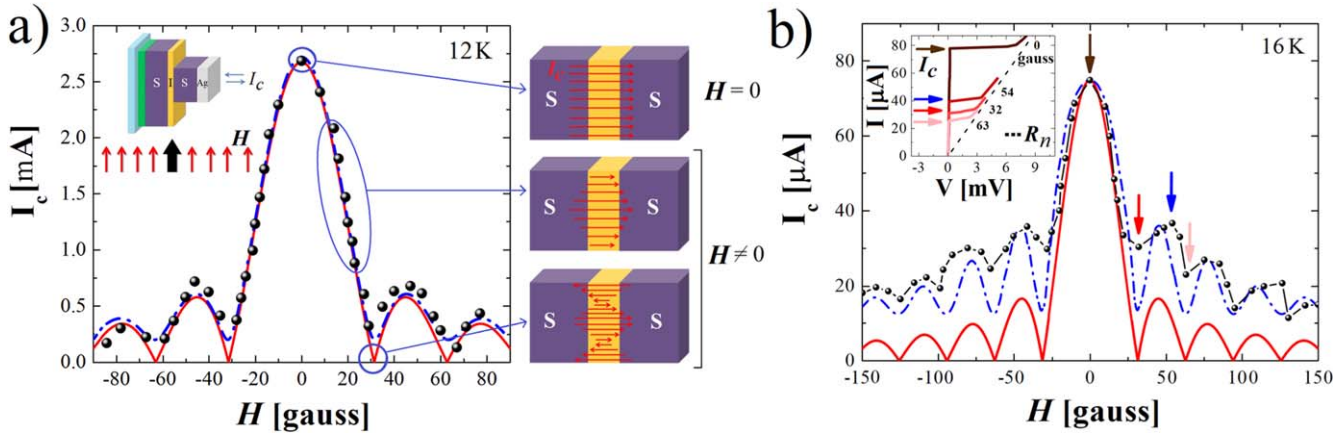

Figure 3. I_c modulation by an external magnetic field for: (a) [G-1-G]; (b) [G-2-G]. The straight and dotted lines correspond to the fit for an ideal JJ using equations (1) and (2), respectively. Inset (a) shows a schematic tunnel junction and the magnetic field configuration. The right part of the panel (a) shows a schematic representation of the effect of the magnetic field on the tunneling currents in a uniform junction. Inset (b) shows typical *I–V* curves obtained at 16 K for different applied magnetic fields. The curves are obtained fixing the magnetic field, applying a current and measuring the voltage.

here $I_0 = J_1 WL$ (J_1 the total current density, W and L the lengths of the junction), H_0 is the value of the magnetic field corresponding to a flux quantum penetrating into the junction. For inhomogeneous barriers with non-zero residual currents where the thickness fluctuations are small in comparison with the thickness of the barrier, the Fraunhofer pattern may be described by [36]

$$I_c(H) = \sqrt{\left(I_0^2 - \frac{\overline{I_1^2}}{\pi N}\right)\left(\frac{\sin\frac{\pi H}{H_0}}{\frac{\pi H}{H_0}}\right)^2 + \frac{\overline{I_1^2}}{\pi N}}, \qquad (2)$$

where $\overline{I_1^2}$ is the mean-square of the current fluctuations across the barrier and N is a factor that represent the thickness fluctuation ($N > 1$ for small fluctuations). The fits for a homogenous (equation (1)) and inhomogeneous (equation (2)) barriers are included in figures 3(a) and (b). The former reproduces the modulations but no the residual current. For the application of equation (2) it is necessary to consider a factor $\gamma^2 = \left(\frac{\overline{I_1^2}}{I_0^2}\right)\left(\frac{1}{\pi N}\right)$. The values of I_c at the minima differ from zero and are γI_o. The data for [G-1-G] and [G-2-G] qualitatively reproduce with $\gamma = 0.083$ and 0.28, respectively. The model considers that residual current at the minima is constant in field. According with the model a large γ corresponds to small N and large thickness fluctuations. The magnetic field dependence of the residual current experimentally observed may be related to large thickness fluctuations and also to a pinhole background.

It is important to mention that the *IV* measurements for [G-3-G] display a different behavior than [G-1-G] and [G-2-G] (see figure 4). No Josephson coupling was observed for this sample, suggesting that the measured superconducting current originates in the electrodes and propagates through pinholes. When the voltage polarization is up, the curves show a step-like transition to a normal state (current is injected from the top to the bottom electrode), however, when the voltage polarization is inverted the normal state remains until a characteristic voltage where a reentrant superconducting state is observed. Suppression of the superconducting state with voltage polarization has been previously observed in superconducting/FE bilayers [37]. It is known that ferroelectricity appears in strained STO [25]. In this scenario, the jumps for the increment / decrement of the resistance could be originated by the switching of the FE domains [38]. The asymmetric properties for the voltage polarization could be related to different T_c for the bottom and top electrodes. Although in [G-3-G] the *IV* curve is dominated by pinholes ($I_p \sim I_c$), the results show that the polarization suppresses the superconducting

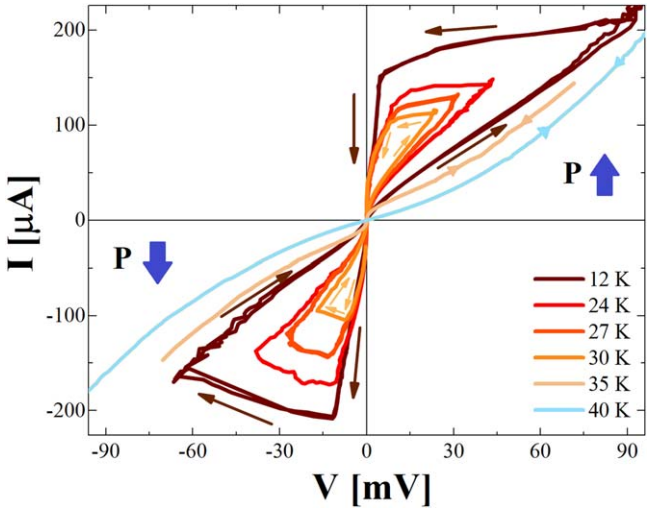

Figure 4. Current versus voltage measurements for [G-3-G] at different temperatures. The arrows indicate the path in which the current is applied. *P* indicates the direction of the polarization (up: from bottom electrode to top electrode; down: from top electrode to bottom electrode). The curves are obtained applying current and measuring voltage. Hysteretic behavior is observed for temperatures below 30 K.

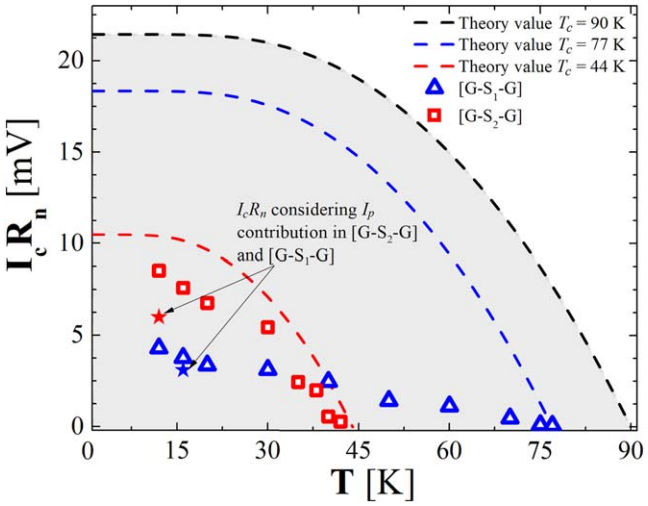

Figure 5. Comparison of I_cR_n measured in [G-1-G] and [G-2-G] with the theoretical expectations according to the equation (2). The dashed lines correspond to the expected values considering T_c of 44, 77 and 90 K.

currents. No features related to changes in the *IV* measurements induced by polarization are observed in [G-4-G].

Figure 5 shows the temperature dependence of I_cR_n for [G-1-G] and [G-2-G]. For SIS with identical superconductors, the theoretical temperature dependence of I_cR_n is limited by the gap as

$$I_cR_n = \frac{\pi\Delta(T)}{2e}\tanh\frac{\Delta(T)}{2kT}, \quad (3)$$

where $\Delta(T) = \Delta(0)\tanh\left\{1.82\left[1.018\left(\frac{T_c}{T}-1\right)\right]^{0.51}\right\}$ [39] and $\Delta(0) = 1.76kT_c$. It is important to note that for *d*-wave superconductors the I_c (T) curves could display a non-monotonic behavior due to changes in the superconducting lobes that contribute to the tunneling [40] (not considered in our analysis). The results show that at 12 K (our lower temperature), the I_cR_n value is strongly affected by the barrier thickness and by the reduction in the T_c of the electrodes. The [G-1-G] displays I_cR_n (12 K) = 4.2 mV and systematically decreases to disappear close to 77 K. [G-2-G] displays I_cR_n (12 K) = 8.9 mV and systematically decreases to disappear at approximately 44 K. The values at 16 K and 12 K subtracting the residual current at the first minima are ~3.1 mV and ~5.7 mV for [G-1-G] and [G-2-G], respectively. A possible explanation for the reduction in its value for [G-1-G] could be related with the barrier uniformity covering the base electrode. A non-uniform covering of the electrode may result in junction areas with thick barrier that does not contribute to the total I_J but provides a resistive shunt to the junction. Moreover, regions with very thin barriers may result in superconductor/normal/superconductor (S/N/S) coupling due to oxygen vacancies [28]. Similar behavior (I_cR_n lower than the theoretical value) has been observed in $MgB_2/TiB_2/MgB_2$ junctions [10]. In our case, the performance of the junction is significantly improved for 2 nm STO barriers where a higher covering of the electrode is expected.

The value of I_cR_n (12 K) ~5.7 mV (subtracting residual current) is larger than that generally observed in NbN [8] and MgB_2 [41] tunnel junctions. For instance, for NbN the theoretical maximum I_cR_n given by the gap is ~4 mV and for MgB_2 junctions the reported values at 4.2 K are ~2 mV [42, 43]. Moreover, the $I_cR_n$values obtained for JJ with ultra-thin barriers are larger than the ones usually observed in ion irradiated YBCO JJ [44, 45]. The large Josephson energy in [G-1-G] and [G-2-G] at low temperatures is evidenced from the *IV* curves with low I_N [11]. Nowadays, with the existence of high-performance cryogenerators, the T_J value is not an issue. Moreover, the quantum effects tend to wash out as a consequence of thermal noise when the operation temperature is increased, which becomes critical for superconducting devices operation. A high Josephson energy is essential for the development of high-quality JJ for two factors, reduced influence of thermal noise and a higher operating frequency.

4. Conclusions

In summary, we have fabricated vertically stacked GBCO/STO/GBCO tunnel junctions with ultra-thin STO barriers. Josephson coupling is observed for GBCO/STO/GBCO tunnel junctions with STO barriers of 1 nm and 2 nm. The I_cR_n values are affected by the presence of pinholes and fluctuations in the barrier thickness. For thin insulator barriers, the presence of short circuits tends to reduce the I_cR_n value. Moreover, S/N/S coupling cannot be discarded. Subtracting the residual current in the Fraunhofer patterns, we obtain I_cR_n (12 K) = 5.7 mV, which is close to the theoretical prediction for JJ with T_c ~ 27 K. The use of thin GBCO electrodes with low surface roughness allowed the fabrication of JJs using very thin insulating barriers. These junctions present high I_cR_n values reducing the thermal noise and increasing the response and frequency operation of the JJs. These are promising results for the development of superconducting devices.

Acknowledgments

This work was partially supported by the ANPCYT (PICT 2015-2171). HN, MS and NH are members of the Instituto de Nanociencia y Nanotecnología CNEA-CONICET (Argentina).

ORCID iDs

H Navarro https://orcid.org/0000-0003-2899-1953
N Haberkorn https://orcid.org/0000-0002-5261-1642

References

[1] Koelle D, Kleiner R, Ludwig F, Dantsker E and Clarke J 1999 High-transition-temperature superconducting quantum interference devices *Rev. Mod. Phys.* **71** 631
[2] Friedrich S 2008 Superconducting tunnel junction photon detectors: theory and applications *J. Low Temp. Phys.* **151** 277–86

[3] Virtanen P, Ronzani A and Giazotto F 2018 Josephson photodetectors via temperature-to-phase conversion *Phys. Rev Appl.* **9** 054027

[4] Mitchell E, Hannam K, Lazar J, Leslie K, Lewis C, Grancea A, Keenan S, Lam S and Foley C 2016 2D SQIF arrays using 20 000 YBCO high R_n Josephson junctions *Supercond. Sci. Technol.* **29** 06LT01

[5] Mukhanov O, Inamdar A, Filippov T, Sahu A, Sarwana S and Semenov V 2007 Superconductor components for direct digital synthesizer *IEEE Trans. Appl. Supercond.* **17** 416–21

[6] Dagan Y, Krupke R and Deutscher G 2000 Determination of the superconducting gap in $YBa_2Cu_3O_{7-\delta}$ by tunneling experiments under magnetic fields *Phys. Rev.* B **62** 146

[7] Lacquaniti V, Andreone D, De Leo N, Fretto M, Sosso A and Belogolovskii M 2009 Engineering overdamped niobium-based josephson junctions for operation above 4.2 K *IEEE Trans. Appl. Supercond.* **19** 234

[8] Wang Z, Terai H, Qiu W, Makise K, Uzawa Y, Kimoto K and Nakamura Y 2013 High-quality epitaxial NbN/AlN/NbN tunnel junctions with a wide range of current density *Appl. Phys. Lett.* **102** 142604

[9] Burnell G, Kang D, Lee H, Moon S, Oh B and Blamire M 2001 Planar superconductor-normal-superconductor Josephson junctions in MgB_2 *Appl. Phys. Lett.* **79** 3464

[10] Galan E, Cunnane D, Xi X X and Chen K 2014 Sandwich-type $MgB_2/TiB_2/MgB_2$ Josephson junctions *Supercond. Sci. Technol.* **27** 065015

[11] Berkowitz S J, Skocpol W J, Mankiewich P M, Ono R H, Missert N, Rosenthal P A and Vale L R 1994 Thermal noise in high-temperature superconducting-normal-superconducting step-edge Josephson junctions *J. Appl. Phys.* **76** 1337

[12] Booij W, Pauza A, Tarte E, Moore D and Blamire M 1997 Proximity coupling in high-T_c Josephson junctions produced by focused electron beam irradiation *Phys. Rev.* B **55** 14600–9

[13] Cybart S, Cho E, Wong T, Wehlin B, Ma M, Huynh C and Dynes R 2015 Nano Josephson superconducting tunnel junctions in $YBa_2Cu_3O_{7-\delta}$ directly patterned with a focused helium ion beam *Nat. Nanotechnol.* **10** 598

[14] Moeckly B and Char K 1997 Properties of interface-engineered high T_c Josephson junctions *Appl. Phys. Lett.* **71** 2526

[15] Oh B, Choi Y, Moon S, Kim H and Min B 1996 $YBa_2Cu_3O_{7-\delta}/NdBa_2Cu_3O_{7-\delta}/YBa_2Cu_3O_{7-\delta}$ edge junctions and SQUIDS *Appl. Phys. Lett.* **69** 2288

[16] Chaudhari P, Mannhart J, Dimos D, Tsuei C C, Chi J, Oprysko M M and Scheuermannn M 1988 Direct measurement of the superconducting properties of single grain boundaries in $Y_1Ba_2Cu_3O_{7-\delta}$ *Phys. Rev. Lett.* **60** 1653

[17] Geerk J, Xi X X and Linker G 1988 Electron tunneling into thin films of $Y_1Ba_2Cu_3O_7$ *Z. Phys.* B **73** 329

[18] Hilgenkamp H and Mannhart J 2002 Grain boundaries in high-T_c superconductors *Rev. Mod. Phys.* **74** 485

[19] Babcock S, Cai X, Kaiser D and Larbalestier D 1990 Weak-link-free behaviour of high-angle $YBa_2Cu_3O_{7-\delta}$ grain boundaries in high magnetic fields *Nature* **347** 167–9

[20] Boris A, Rydh A, Golod T, Motzkau H, Klushin A and Krasnov V 2013 Evidence for nonlocal electrodynamics in planar josephson junctions *Phys. Rev. Lett.* **111** 117002

[21] Verhoeven M A J, Gerritsma G J, Rogalla H and Golubov A 1995 Ramp type HTS Josephson junctions with PrBaCuGaO barriers *IEEE Trans. Appl. Supercond.* **5** 2095

[22] Navarro H, Sirena M, Kim J and Haberkorn N 2015 Smooth surfaces in very thin $GdBa_2Cu_3O_{7-\delta}$ films for application in superconducting tunnel junctions *Physica* C **510** 21–6

[23] Garcia-Barriocanal J, Perez-Munoz A M, Sefrioui Z, Arias D, Varela M, Leon C, Pennycook S J and Santamaria J 2013 Disorder-controlled superconductivity at $YBa_2Cu_3O_7/SrTiO_3$ interfaces *Phys. Rev.* B **87** 245105

[24] Muller K A and Burkard H 1979 $SrTiO_3$: an intrinsic quantum paraelectric below 4 K *Phys. Rev.* B **19** 3593

[25] Haeni J *et al* 2004 Room-temperature ferroelectricity in strained $SrTiO_3$ *Nature* **430** 758–61

[26] Navarro H, Sirena M, González J, Troiani H, del Corro P, Granell P, Golmar F and Haberkorn N 2018 Electrical transport across nanometric $SrTiO_3$ and $BaTiO_3$ barriers in conducting/insulator/conducting junctions *Mater. Res. Express* **5** 016408

[27] Haberkorn N, Lovey F, Condó A M and Guimpel J 2005 High-resolution transmission electron microscopy study of the interfaces and stacking defects in superconducting/magnetic perovskite superlattices *J. Appl. Phys.* **97** 053511

[28] Kun L, Zheng W, Di W, Haifa Z and Aidong L 2013 Bipolar resistive switching based on $SrTiO_3/YBa_2Cu_3O_7$ epi-layers *J. Phys. D: Appl. Phys.* **46** 035308

[29] Sirena M, Avilés L and Haberkorn N 2013 High transition temperature superconductor/insulator bilayers for the development of ultra-fast electronics *Appl. Phys. Lett.* **103** 052902

[30] Navarro H, Yang I, Sirena M, Kim J and Haberkorn N 2015 Characterization of the insulator barrier and the superconducting transition temperature in $GdBa_2Cu_3O_{7-d}/BaTiO_3$ bilayers for application in tunnel junctions *J. Appl. Phys.* **118** 45308

[31] Wuyts B, Moshchalkov V and Bruynseraede Y 1996 Resistivity and Hall effect of metallic oxygen-deficient $YBa_2Cu_3O_x$ films in the normal state *Phys. Rev.* B **53** 9418

[32] Kroger H 1980 *US Patent* US4421785Assignee to Sperry Corporation, New York

[33] Blatter G, Feigelman M V, Geshkenbein V G, Larkin A I and Vinokur V M 1994 Vortices in high-temperature superconductors *Rev. Mod. Phys.* **66** 1125

[34] Baumert B A, Talvacchio J and Forrester M G 1993 $SrTiO_3$ buffer layers and tunnel barriers for Ba-K-Bi-O junctions *Appl. Phys. Lett.* **62** 2137

[35] Barone A and Paterno G 1982 *Physics and Applications of the Josephson Effect* (New York: Wiley) p 90

[36] Yanson I K 1970 Effect of fluctuations on the dependence of the Josephson current on the magnetic field *Sov. Phys.—JETP* **31** 800

[37] Crassous A, Bernard R, Fusil S, Bouzehouane K, Le Bourdais D, Enouz-Vedrenne S, Briatico J, Bibes M, Barthélémy A and Villegas J 2011 Nanoscale electrostatic manipulation of magnetic flux quanta in ferroelectric/superconductor $BiFeO_3/YBa_2Cu_3O_{7-\delta}$ heterostructures *Phys. Rev. Lett.* **107** 247002

[38] Kohlstedt H, Pertsev N, Rodríguez J and Waser R 2005 Theoretical current–voltage characteristics of ferroelectric tunnel junctions *Phys. Rev.* B **72** 125341

[39] Carrington A and Manzano F 2003 Magnetic penetration depth of MgB_2 *Physica* C **385** 205–14

[40] Gabovich A and Voitenko A 2014 Anomalous temperature dependence of the stationary Josephson tunnel current in junctions between d-wave superconductors *Low Temp. Phys.* **40** 816

[41] Burnell G, Kang D, Lee H, Moon S, Oh B and Blamire M 2001 Planar superconductor-normal-superconductor Josephson junctions in *Appl. Phys. Lett.* **79** 3464

[42] Ke C, Zhuang C G, Li Qi, Zhu Y, Voyles P M, Weng X, Redwing J M, Singh R K, Kleinsasser A W and Xi X X 2010 High-J_c MgB_2 Josephson junctions with operating temperature up to 40 K *Appl. Phys. Lett.* **96** 042506

[43] Cui Y, Chen Ke, Qi L, Xi X X and Rowell J M 2006 Degradation-free interfaces in MgB_2/insulator/Pb Josephson tunnel junctions *Appl. Phys. Lett.* **89** 202513

[44] Bergeal N, Lesueur J, Sirena M, Aprili M, Contour J and Leridon B 2007 Using ion irradiation to make high-T_c Josephson junctions *J. Appl. Phys.* **102** 083903

[45] Mitchell E and Foley C 2010 YBCO step-edge junctions with high I_cR_n *Supercond. Sci. Technol.* **23** 065007